Experimental Investigation of the Effect of Wave-Current Interactions on the Morphology and Dynamics of Subaqueous Dunes

Iskander Abroug, Pierre Weill, Nizar Abcha

▶ **To cite this version:**

Iskander Abroug, Pierre Weill, Nizar Abcha. Experimental Investigation of the Effect of Wave-Current Interactions on the Morphology and Dynamics of Subaqueous Dunes. Journal of Geophysical Research: Earth Surface, 2025, 130 (6), pp.e2023JF007623. ⟨10.1029/2023JF007623⟩. ⟨hal-05106684⟩

HAL Id: hal-05106684

https://normandie-univ.hal.science/hal-05106684v1

Submitted on 11 Jun 2025

HAL is a multi-disciplinary open access archive for the deposit and dissemination of scientific research documents, whether they are published or not. The documents may come from teaching and research institutions in France or abroad, or from public or private research centers.

L'archive ouverte pluridisciplinaire **HAL**, est destinée au dépôt et à la diffusion de documents scientifiques de niveau recherche, publiés ou non, émanant des établissements d'enseignement et de recherche français ou étrangers, des laboratoires publics ou privés.

Copyright - All rights reserved

Check for updates

JGR Earth Surface

RESEARCH ARTICLE
10.1029/2023JF007623

Special Collection:
Marine and River Dune Dynamics

Experimental Investigation of the Effect of Wave-Current Interactions on the Morphology and Dynamics of Subaqueous Dunes

I. Abroug[1], P. Weill[1], and N. Abcha[1]

[1]Normandie Université, UNICAEN, UNIROUEN, CNRS, UMR 6143 M2C, Caen, France

Key Points:

- The dune height and wavelength are found to decrease linearly as the wave steepness increases
- The time needed for the dunes to reach an equilibrium morphology decreases with increasing combined flow velocity
- Non-Gaussian statistics for horizontal velocity field are generated by the bathymetric changes along the dune profile

Correspondence to:
I. Abroug,
iskander.abroug@unicaen.fr

Citation:
Abroug, I., Weill, P., & Abcha, N. (2025). Experimental investigation of the effect of wave-current interactions on the morphology and dynamics of subaqueous dunes. *Journal of Geophysical Research: Earth Surface*, *130*, e2023JF007623. https://doi.org/10.1029/2023JF007623

Received 5 JAN 2024
Accepted 3 APR 2025

Author Contributions:
Conceptualization: I. Abroug, P. Weill
Data curation: I. Abroug
Funding acquisition: P. Weill, N. Abcha
Investigation: I. Abroug
Methodology: I. Abroug, P. Weill
Project administration: P. Weill, N. Abcha
Supervision: P. Weill, N. Abcha
Visualization: I. Abroug
Writing – original draft: I. Abroug
Writing – review & editing: I. Abroug, P. Weill, N. Abcha

© 2025. American Geophysical Union. All Rights Reserved.

Abstract Dunes in natural marine environments are subject to various complex and unsteady hydrodynamic forcings. In shallow waters and intertidal environments in particular, subaqueous dunes are strongly influenced by waves which combine with unidirectional or reversing currents. Understanding and predicting their morphology and dynamics is crucial because bedform-related roughness strongly influences sediment transport. In this article, we investigate in a flume tank the impact of monochromatic waves combined with a unidirectional current on the geometry of migrating dunes as well as the associated flow field. The influence of the wave steepness and dispersion on the bathymetry temporal evolution, the streamwise velocity, the vertical velocity, the turbulence intensity, and Reynolds shear stress above migrating dunes were examined. Furthermore, higher order moments related to the streamwise velocity were calculated in order to evaluate the flow non-Gaussian behavior above migrating dunes. Our experiments confirm that the presence of migrating dunes can produce non-Gaussian statistics related to the streamwise velocity. The skewness and the kurtosis of the horizontal velocity have different trends. Skewness has a local maximum on the top of the stoss shallower region of the dune, whereas the kurtosis has a local maximum on the dune's lee side.

Plain Language Summary Dunes in natural marine environments are subject to various complex and unsteady hydrodynamic forcings. In shallow waters and intertidal environments in particular, subaqueous dunes are strongly influenced by waves which combine with unidirectional or reversing currents. The present study has focused on the topography temporal evolution and on the details of flow above migrating dunes in equilibrium in the presence of combined flows.

1. Introduction

In general, subaqueous ripples and dunes in riverine and marine environments result from the instability mechanism related to the lag between bed elevation, bed shear stress and sediment transport (Fouriere et al., 2010). On the one hand, the flow around ripples is not affected by the water surface because their wavelength λ is significantly smaller than the water depth h. On the other hand, dunes interact with the free surface because their mean wavelength is equal to or greater than h. Previously thought to be two different modes of the same linear instability, dunes are now thought to be caused by ripples becoming coarser due to a nonlinear rise in their wavelength (Andreotti et al., 2012). Starting from a flat bed, ripples first emerge at a small wavelength and then develop in height and quickly reach the aspect ratio where the turbulent boundary layer splits from the bed, creating a recirculation bubble and an avalanche slip face. Duràn et al. (2019) demonstrated that, depending on both, Reynolds number $\left(R_\lambda = u_*\lambda/\nu\right.$ where λ is the bed wavelength, u_* is the shear velocity of the flow and ν its kinematic viscosity$\left.\right)$ and grain-based Reynolds number $\left(R_d = u_* d/\nu\right.$, where d is the grain size$\left.\right)$, the final pattern corresponds to mature ripples, smooth dunes or dunes with superimposed ripples, as observed in natural and laboratory conditions (Figure 2 in Duràn et al., 2019). In other words, the final pattern is associated with the inner boundary layer (from viscous to inertial to turbulent dominated regimes as R_λ increases), which varies according to the bedform surface's hydrodynamic roughness as determined by R_d.

Subaqueous dunes or megaripples are prevalent bedforms in fluvial and marine environments where relatively coarse sediments (from medium sand to gravel) are exposed to strong subcritical flows (Ashley, 1990; Southard & Boguchwal, 1990). In tide-dominated shelves, these bedforms are often superimposed on larger sedimentary bodies such as sandwaves and tidal banks (e.g., Jones & Traykovski, 2019). Bed roughness generated by dunes and megaripples increases flow resistance (e.g., Engel & Lau, 1980) and turbulent intensity (e.g., Best, 2005), and

21699011, 2025, 6, Downloaded from https://agupubs.onlinelibrary.wiley.com/doi/10.1029/2023JF007623 by Universitaet De Caen Normandie, Wiley Online Library on [10/06/2025]. See the Terms and Conditions (https://onlinelibrary.wiley.com/terms-and-conditions) on Wiley Online Library for rules of use; OA articles are governed by the applicable Creative Commons License

subsequently exert a significant influence on local hydrodynamics and sediment transport processes. Understanding the morphology and dynamics of subaqueous dunes is therefore essential for accurate predictions of flow patterns, sediment fluxes, and bathymetric changes. As coastal regions witness a surge in offshore activities, our ability to predict large subaqueous bedform dynamics holds crucial implications for coastal management, offshore renewable energy production (e.g., Barrie & Conway, 2014; Couldrey et al., 2020) navigation (Whitmeyer & Fitzgerald, 2006), and the sustainable development of marine resources (e.g., Lancker et al., 2020).

In shallow tide-dominated shelves, including estuaries or intertidal sand flat environments, subaqueous dunes (or megaripples) are subject to varying flow conditions and wave-current interactions. Contrary to larger bedforms, their sizes are sufficiently small to adapt their morphology to transient flow conditions within a time-span of several hours to a few days. Scaling relations of dunes and the control of hydrodynamics on dune geometry in pure unidirectional currents are now quite well constrained, although a significant degree of scatter in field and experimental data arises due to natural variability (Bradley & Venditti, 2017). However, we know very little about how surface waves impact these bed features.

Physical experiments have been and remain a practical tool to investigate sediment transport processes as well as the development and stability of bedforms (Southard, 1991). To date, most of the flume experiments conducted on subaqueous dunes have been performed under unidirectional steady current (Blom et al., 2003; Bridge & Best, 1988; Kleinhans, 2004; Naqshband et al., 2014; Schindler & Robert, 2005; Southard & Boguchwal, 1990; Vah et al., 2020; Venditti et al., 2005; Warmink, 2014; Wren et al., 2007), and studies dealing with combined flows (i.e., waves and current interactions) are scarce. However, according to Singh et al. (2018), surface waves are known to alter the mean flow and turbulence field, which in turn affects flow resistance, sediment transport, and momentum transfer.

Thirty years ago, Yokokawa et al. (1995) were among the first to explore the dynamics of ripples under the action of combined flow. They demonstrated that small vortices generated by low oscillatory flow velocity result in rounded ripples, whereas greater oscillatory flow velocity yields bigger vortices and more acute crests. Arnott and Southard (1990) and Dumas and Arnott (2006) performed similar experiments in order to define equilibrium combined-flow bed configurations under a wide range of oscillatory and unidirectional velocity components. They found that pure oscillatory flows should be responsible for forming hummocky cross-stratifications described in fossil sediment deposits. Catano-Lopera and Garcia (2006) generated sandwaves (fine to medium sand, wavelength between 2 and 8 m) with superimposed ripples under combined flow conditions. Although the relationships between sandwave morphology and hydrodynamics show a large degree of scatter, it appears that sandwave length and height decrease and sandwave migration speed increases as the wave Reynolds number increases. Chatterjee et al. (2018) investigated the influence of a counter-current on wave propagation and resulting wave-generated bedforms (ripples). Perillo et al. (2014) investigated the stability and geometry of small-scale bedforms (ripples—wavelength in the order of 10^{-1} m) under long-period oscillating and combined flows in a water tunnel, with a focus on the development path toward the equilibrium morphology. To date, there is still a need to explore how dunes grow in the presence of currents interacting with short-period waves, and to understand how waves modify the dune morphology in comparison with current-only dynamic equilibrium morphology. Widening the range of grain-size and hydrodynamic conditions is also essential to build a large experimental data set and strengthen empirical models of bedform development.

In the present study, we examine in a 16 m-long wave and current flume the formation, dynamics and equilibrium morphology of coarse-grained, current-dominated dunes influenced by waves, by exploring a range of wave period and amplitude values. In order to gain insight into the relationships between bed forms and turbulence patterns, bathymetric measurements are performed at regular intervals throughout the experiments, and velocity profiling above the migrating dunes is performed together with free-surface measurements. The analysis of the velocity profiles in terms of statistical moments (skewness and kurtosis) allows to emphasize the influence of superimposed waves and bed topography on the streamwise velocity field.

2. Materials and Methods

Experiments were carried out in the wave and current flume of the M2C laboratory located in Caen Normandy University (France). The flume is 16 m long, 0.5 m wide and 0.5 m deep, and is equipped with a piston type wave maker and a centrifugal pump for water recirculation (Figure 1). Waves of different spectra and amplitudes can be generated in the flume under conditions of deep and shallow water.

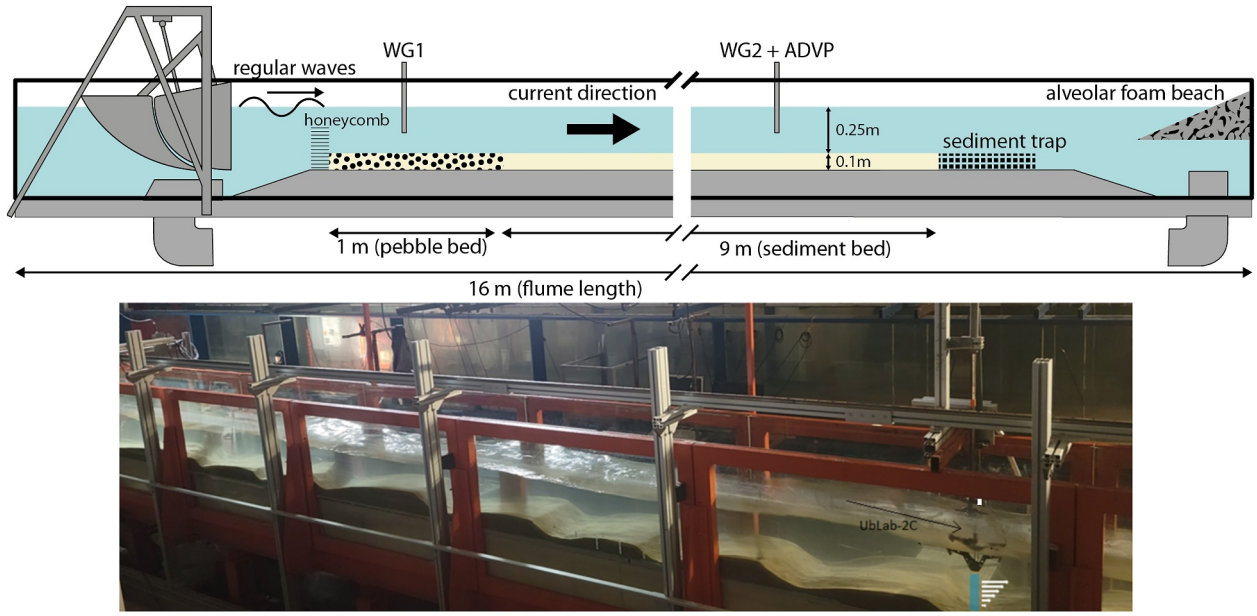

Figure 1. Top: sketch view of the wave and current flume. Bottom: developed dune field along the effective measurement section of the flume. Water and waves are from left to right.

Based on the bedform phase diagram of Southard and Boguchwal (1990), a coarse siliceous sand with a median diameter D_{50} of 573 μm (0.81 ϕ) and a density s = ρ_s/ρ of 2.65 is chosen for the experiments. The grainsize distribution is symmetrical (skewness Sk = −0.07 ϕ) and the sand is moderately well sorted with a sorting parameter σ of 0.52 ϕ (logarithmic method of moments, Blott & Pye, 2001). A 10 cm-thick sand bed is installed over 9 m along the 12 m-long test section of the flume and flattened at the beginning of each test. Upstream of the sediment bed, a 20 cm-high honeycomb was installed in order to break down large-scale turbulence generated by the pump. It is followed by a 1 m-long pebble bed to ensure the fast development of a turbulent boundary layer. An alveolar foam beach is installed at the downstream end of the flume to prevent wave reflection.

At the beginning of each test, the flume is slowly filled with water up to a water depth h of 25 cm above the sand bed. A flow velocity of 0.5 m/s is adopted, resulting in a Froude number $\boldsymbol{Fr} = \frac{U}{\sqrt{gh}} = \mathbf{0.32}$, and monochromatic waves are generated for combined flow experiments. Every 15 min, both wave and current generators are stopped in order to proceed to the bathymetric measurements, and to recirculate upstream the bedload collected downstream of the test section in a sediment trap.

The bed topography was monitored over the 9 m-long effective measurement section using a laser distance-meter (SICK-DT500, Waldkirch, Germany) mounted on the carriage. The uncertainty of the distance measurement is 3 mm. Five parallel transects over the flume width were acquired, allowing the reconstruction of the 3D bed surface by interpolation. The bedform tracking tool (Van der Mark & Blom, 2007; Van der Mark et al., 2008) was applied to each of the five individual topographic profiles and used to derive the mean bedform characteristics (height Δ and wavelength λ) and to quantify their variability. This method consists of determining zero upcrossings and zero downcrossings in the detrended bed elevation profiles to identify the bedform crests (maximum value between a zero up- and zero downcrossing) and troughs (minimum value between a zero down- and zero upcrossing). The bedform height Δ and length λ are defined as the vertical distance between the crest and downstream trough, and the horizontal distance between two consecutive crests. These two geometrical parameters are determined using the five parallel transect across the entire bed to calculate the mean geometric parameters. Tests were performed using crest to upstream trough distance and trough to trough distance for bedform height and length calculation, respectively, and led to negligible differences. A wavelet-based bispectral analysis has also been used to determine dune geometrical parameters (Catano-Lopera et al., 2009), showing non-significant differences. Finally, employing multiple definitions did not significantly increase the signal-to-noise ratio. It appears that the scatter of the dune geometric parameters is more likely related to natural variability rather than method-dependent uncertainties.

21699011, 2025, 6, Downloaded from https://agupubs.onlinelibrary.wiley.com/doi/10.1029/2023JF007623 by Universitaet De Caen Normandie, Wiley Online Library on [10/06/2025]. See the Terms and Conditions (https://onlinelibrary.wiley.com/terms-and-conditions) on Wiley Online Library for rules of use; OA articles are governed by the applicable Creative Commons License

21699011, 2025, 6, Downloaded from https://agupubs.onlinelibrary.wiley.com/doi/10.1029/2023JF007623 by Universitaet De Caen Normandie, Wiley Online Library on [10/06/2025]. See the Terms and Conditions (https://onlinelibrary.wiley.com/terms-and-conditions) on Wiley Online Library for rules of use; OA articles are governed by the applicable Creative Commons License

Table 1
Summary of Flow Waves and Dune Development Characteristics

Test	Description	U [m/s]	f [Hz]	ε	S	kh	U_{wm} [m/s]	U_{cf} [m/s]	C [m/h]
T_A	PUF	0.5	--	--	--		--	0.5	2.56
T_{A1}	CF—low	0.5	0.5	0.05	2.70	0.52	0.08	0.58	1.66
T_{A2}	CF—intermediate	0.5	0.5	0.07	2.79	0.52	0.11	0.61	2.37
T_{A3}	CF—high	0.5	0.5	0.11	5.95	0.52	0.18	0.68	2.81
T_{A4}	CF—low	0.5	0.75	0.06	6.85	0.83	0.10	0.60	2.44
T_{A5}	CF—intermediate	0.5	0.75	0.1	11.43	0.83	0.16	0.66	2.88
T_{A6}	CF—high	0.5	0.75	0.14	16.00	0.83	0.23	0.73	3.2
T_{A7}	CF—low	0.5	1	0.06	17.28	1.20	0.10	0.60	2.04
T_{A8}	CF—intermediate	0.5	1	0.11	31.68	1.20	0.17	0.67	2.22
T_{A9}	CF—high	0.5	1	0.14	40.32	1.20	0.23	0.73	2.36

Note. PUF, pure unidirectional flow; CF, combined flow; U, the unidirectional current velocity; U_{wm}, the maximum orbital velocity; $U_{cf} = U + U_{wm}$, the combined flow velocity; C, the dune equilibrium migration speed.

Furthermore, velocity profiles were acquired on the downstream part of the sediment bed once the dunes reached a dynamic equilibrium (relative stability of bedform wavelength and height). A downward-looking acoustic Doppler velocity profiler (UB-Lab 2C, UBERTONE, Schiltigheim, France) was used to measure two co-located vertical velocity profiles of the streamwise (u) and vertical (w) velocity components. The UB-Lab 2C, with a carrier frequency of 1 MHz, is set to measure 17 cm-long profiles with a bin resolution of 3 mm. The estimation of the velocity requires a coherent Doppler phase evolution between two consecutive pulses and this can be insured with a high Pulse Repetition Frequency (PRF) of 900 Hz. A single measurement is obtained by the mean of 45 samples at the PRF frequency, resulting in an acquisition frequency f_{acq} of 20 Hz. The distance between the probe and the sediment bed is retrieved from the maximum echo intensity of the backscattered signal.

In addition to topography and flow measurements, the temporal variation of the free surface elevation was monitored using two resistive wave gauges with a sampling frequency of 100 Hz. A first wave gauge (WG1) was fixed at a distance of 1 m from the wave maker to determine the input wave parameters. The second one (WG2) was positioned in close proximity to the UB-Lab 2C device at a distance of about 9 m from the wave maker to monitor the wave characteristics modified by the bed topography.

The first experiment was set using a pure unidirectional current of 0.5 m/s and a water depth h of 0.25 m. Based on this reference current velocity, nine combined flow experiments were performed with wave frequency f of 0.5, 0.75 and 1 Hz, and wave steepness $\varepsilon = a/h \in [0.05 : 0.14]$. The maximum orbital velocity U_{wm} is calculated using Equation 1 (Wiberg & Sherwood, 2008).

$$U_w = \omega a \frac{\cosh k(h+z)}{\sinh(kh)} \tag{1}$$

where U_w represents the orbital velocity at a given water depth, $\omega = 2\pi/f$ denotes the wave pulsation and k is the wavenumber calculated using the linear dispersion relation $\omega^2 = g.k.\tanh(kh)$. Wave parameters were chosen relative to the mean water depth in order to obtain an intermediate water depth configuration ($0.5 < kh < 2$) where wave orbitals have an influence on the sediment bed ($h < L/2$; Wiberg & Sherwood, 2008). The different test configurations are summarized in Table 1.

3. Results

3.1. Bathymetry Temporal Evolution

The formation of dunes from an initially flat bed and their temporal evolution were investigated for the 10 experimental configurations reported in Table 1. An example of the bathymetry temporal evolution in a combined flow condition (Test TA4) is shown in Figure 2a. After 15 min, two-dimensional ripples form from the initial flat

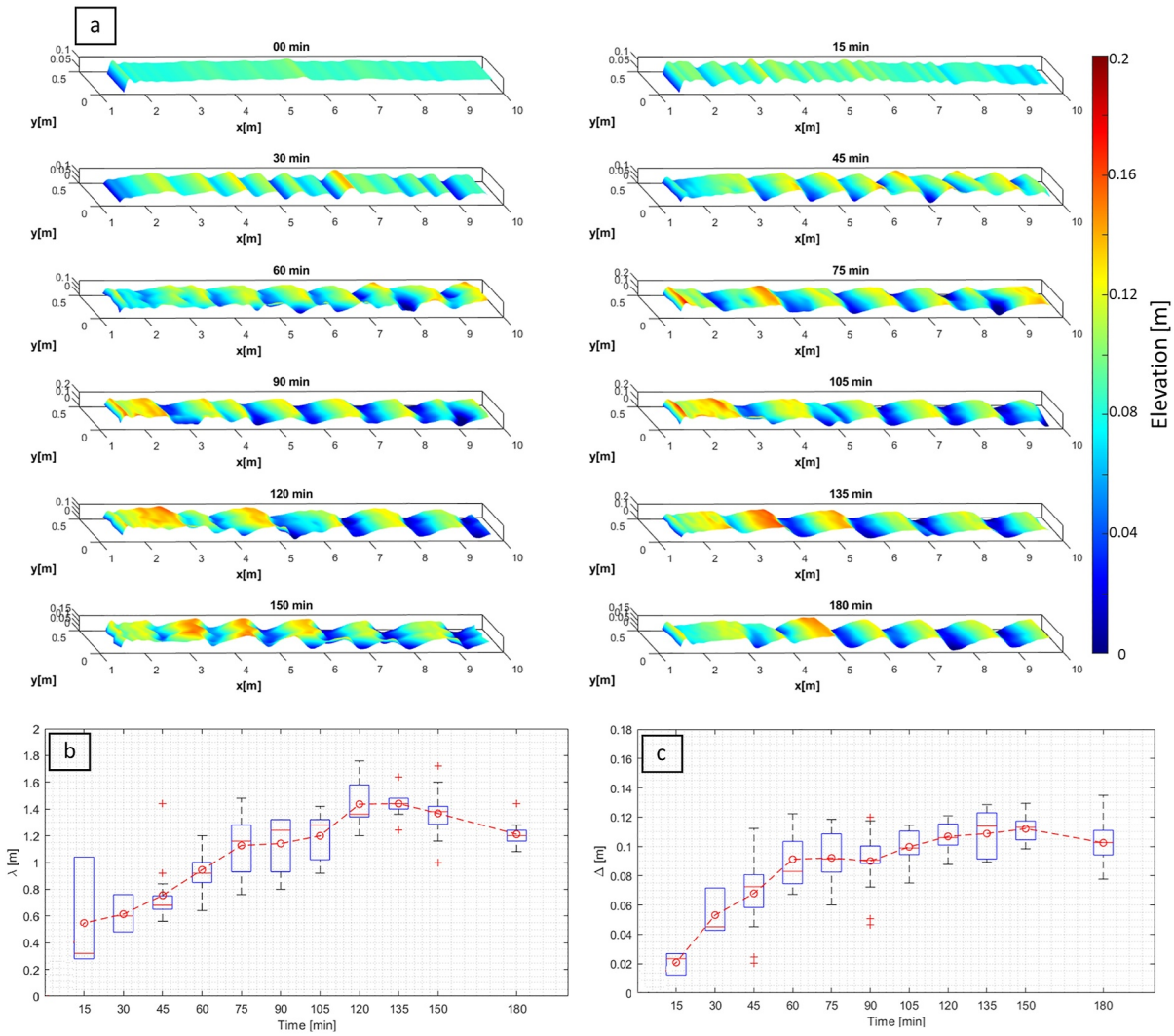

Figure 2. (a) Temporal evolution of the bed elevation (relative to the flume hard bottom) in the presence of a combined flow (Test T_{A4}). (b, c) Temporal evolution of the dune wavelength and amplitude, respectively. The flow and the wave propagation are from left to right. On each box, the horizontal red line depicts the median, and the bottom and top edges of the box represent the 25th and 75th percentiles, respectively. The whiskers, or horizontal lines that extend below and above the boxplot, have endpoints that correspond to the highest and lowest values. The outliers are plotted individually using "+" marker symbol. An outlier is a value that is more than 1.5 times the interquartile range away from the bottom or top of the boxplot.

bed. This observation is consistent with experimental findings obtained in the case of current-dominated combined-flows in Perillo et al. (2014). Thirty minutes later, these two-dimensional ripples start to evolve into two-dimensional dunes by amalgamation. Figures 2b and 2c represent the temporal evolution of the dune wavelength and height during 3 hr of measurements. The mean amplitude and wavelength of the dunes stabilizes some 60 min after the beginning of the experiment. From 60 min, the number of dunes is relatively stable, oscillating between 6 and 7 using splitting and amalgamation processes.

Figure 3 summarizes the temporal evolution of the dune wavelength and amplitude for all studied cases. It is found that the development path of bedform growth exhibits the same general trend regardless of the hydrodynamic conditions. Once the equilibrium stage is achieved, the temporal evolution shows a typical asymptomatic increase and the wavelength λ and dune height Δ fluctuate around their equilibrium values. Non-linear fits for (a) high wave amplitude (CF—high), (b) intermediate wave amplitude (CF—intermediate), and (c) low wave amplitude (CF—low) are shown, respectively, by solid, dashed, and dotted lines. These correlations were obtained using Equations 3 and 4 established by Baas (1993) and used later in Perillo et al. (2014):

21699011, 2025, 6, Downloaded from https://agupubs.onlinelibrary.wiley.com/doi/10.1029/2023JF007623 by Universitaet De Caen Normandie, Wiley Online Library on [10/06/2025]. See the Terms and Conditions (https://onlinelibrary.wiley.com/terms-and-conditions) on Wiley Online Library for rules of use; OA articles are governed by the applicable Creative Commons License

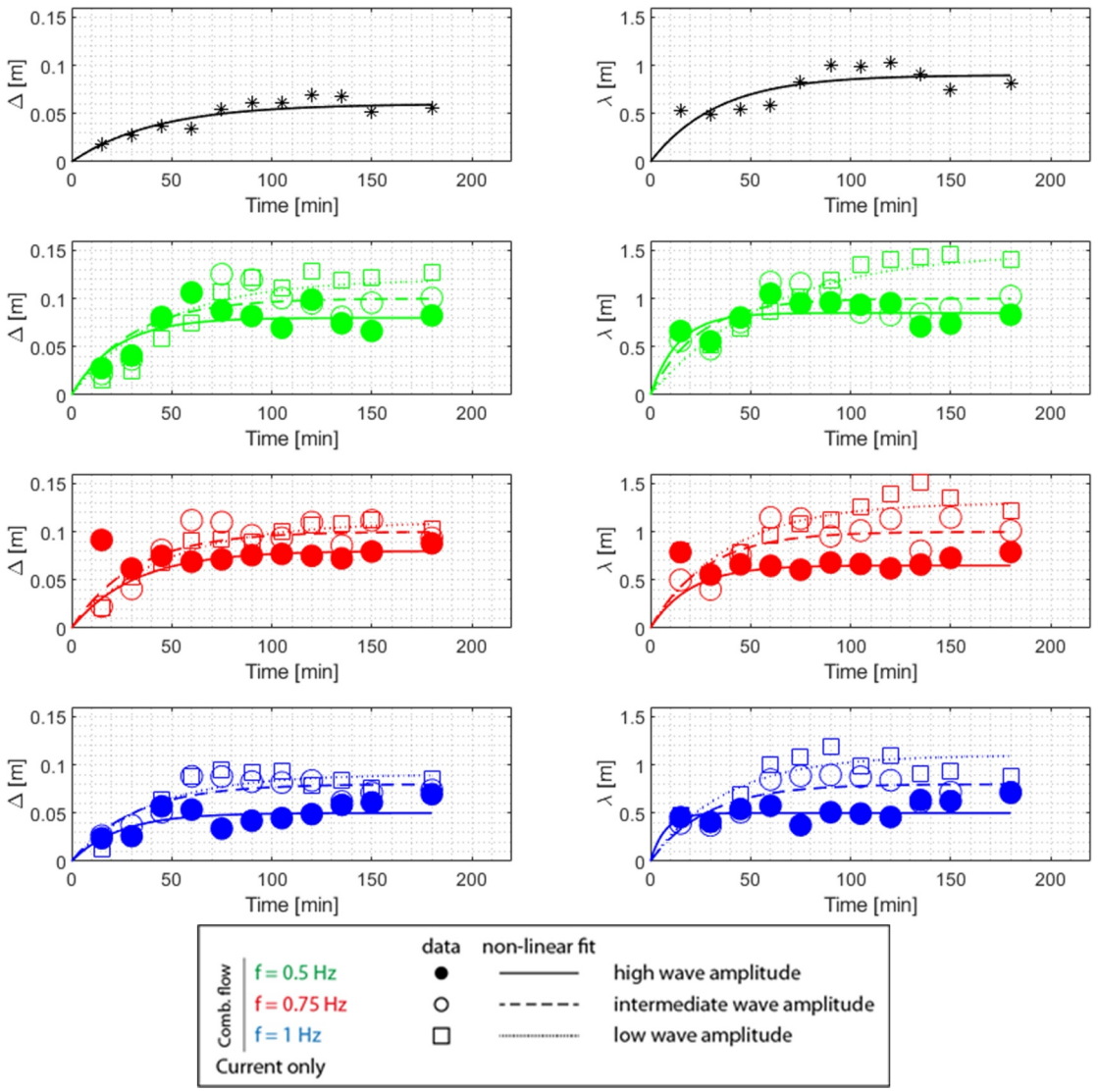

Figure 3. Temporal evolution of dune amplitude and wavelength for all tests. Filled circles, empty circles and empty squares represent, respectively (1) high wave amplitude CF—high (2) intermediate wave amplitude CF—intermediate and (3) low wave amplitude CF—low. Solid, dashed and dotted lines represent non-linear fits for (1) high wave amplitude CF—high (2) intermediate wave amplitude CF—intermediate and (3) low wave amplitude CF—low.

$$\lambda_t(t) = \lambda_{eq}\left(1 - e^{-\alpha_\lambda t}\right) \tag{2}$$

$$\Delta_t(t) = \Delta_{eq}\left(1 - e^{-\alpha_\Delta t}\right) \tag{3}$$

The bedform wavelength and height constants α_λ and α_Δ are optimized using the least absolute residual approach and t represents the elapsed time in minutes. The subscripts (t) and (e) depict actual and equilibrium values. Several definitions are given in previous studies to calculate the equilibrium time. In the present work, the definition given in Perillo et al. (2014) is adopted:

$$t_{eq} = -0.5\left(\frac{\ln(0.1)}{\alpha_\lambda} + \frac{\ln(0.1)}{\alpha_\Delta}\right) \tag{4}$$

Table 2 summarizes different values of λ_{eq}, Δ_{eq}, α_λ, α_Δ, t_{eq} and R^2 the square of the sample correlation coefficient for different studied tests.

21699011, 2025, 6, Downloaded from https://agupubs.onlinelibrary.wiley.com/doi/10.1029/2023JF007623 by Universitaet De Caen Normandie, Wiley Online Library on [10/06/2025]. See the Terms and Conditions (https://onlinelibrary.wiley.com/terms-and-conditions) on Wiley Online Library for rules of use; OA articles are governed by the applicable Creative Commons License

21699011, 2025, 6, Downloaded from https://agupubs.onlinelibrary.wiley.com/doi/10.1029/2023JF007623 by Universitaet De Caen Normandie, Wiley Online Library on [10/06/2025]. See the Terms and Conditions (https://onlinelibrary.wiley.com/terms-and-conditions) on Wiley Online Library for rules of use; OA articles are governed by the applicable Creative Commons License

Table 2
Summary of the Equilibrium Parameters

Test	Description	λ_{eq} [m]	Δ_{eq} [m]	α_λ	α_Δ	t_{eq} [min]	R_α^2	R_β^2
T_A	PUF	0.9	0.06	0.030	0.024	86	0.82	0.89
T_{A1}	CF—low	1.48	0.12	0.017	0.023	118	0.93	0.9
T_{A2}	CF—intermediate	1	0.10	0.042	0.033	61	0.78	0.8
T_{A3}	CF—high	0.85	0.08	0.072	0.045	41	0.81	0.77
T_{A4}	CF—low	1.3	0.11	0.026	0.022	96	0.86	0.98
T_{A5}	CF—intermediate	1	0.1	0.037	0.032	67	0.82	0.85
T_{A6}	CF—high	0.65	0.08	0.05	0.032	59	0.87	0.85
T_{A7}	CF—low	1.1	0.09	0.027	0.026	86	0.83	0.86
T_{A8}	CF—intermediate	0.8	0.08	0.035	0.032	68	0.81	0.84
T_{A9}	CF—high	0.5	0.05	0.138	0.042	35	0.69	0.71

Figure 4 illustrates the time needed to reach the dune equilibrium as a function of the combined flow velocity U_{cf}. Perillo et al. (2014) provided data on asymmetric dunes, which are represented by the blue filled circles. Equation 5, with a correlation coefficient $R^2 = 0.7$, illustrates the nonlinear fit proposed for our experimental data through the solid red line. For the experimental data from Perillo et al. (2014), a second nonlinear fit (Equation 6) is suggested for a variety of bedform types, such as symmetrical ripples, asymmetrical ripples, asymmetrical dunes, and current ripples. Based on the overall data in Figure 4, dunes reach equilibrium faster for higher combined flow velocities, which can be explained by the increased amount of mobilized sediment.

$$U_{cf} = 0.384 t_{eq}^{-0.332} + 0.274 \quad (5)$$

$$U_{cf} = 0.251 t_{eq}^{-0.332} + 0.351 \quad (6)$$

where t_e[hr] is the time needed to reach the equilibrium, $m(s.h)^{-1}$ is the unit of the first constant in both equations and m/s is the unit of the second constant.

Figure 5 shows the equilibrium dune height Δ_{eq} and wavelength λ_{eq} against the wave nonlinearity ε. Linear fit on the acquired data is shown by the black dotted line. The two geometric parameters, dune wavelength λ_{eq} and

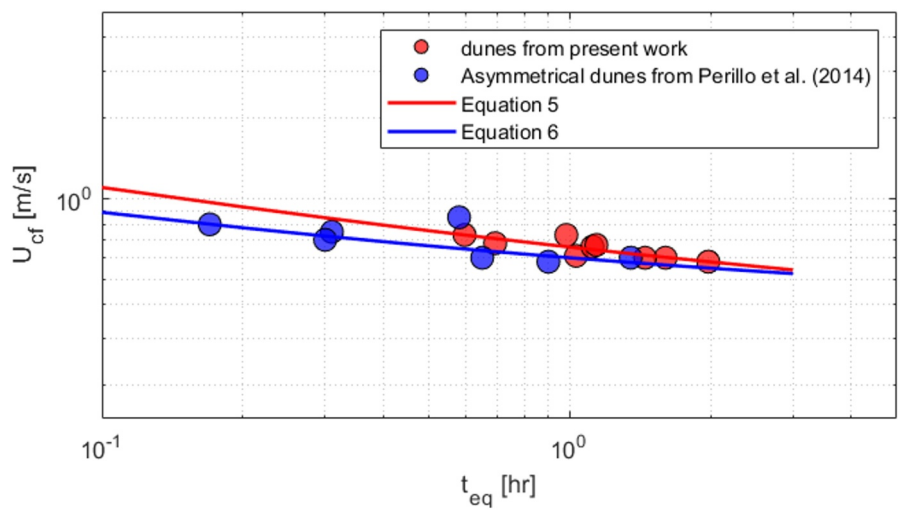

Figure 4. Equilibrium time for dune development as a function of U_{cf}. Blue filled circles correspond to asymmetrical dune data taken from Perillo et al. (2014) and red filled circles represent experimental data of the present study. The two solid lines correspond to Equations 5 and 6.

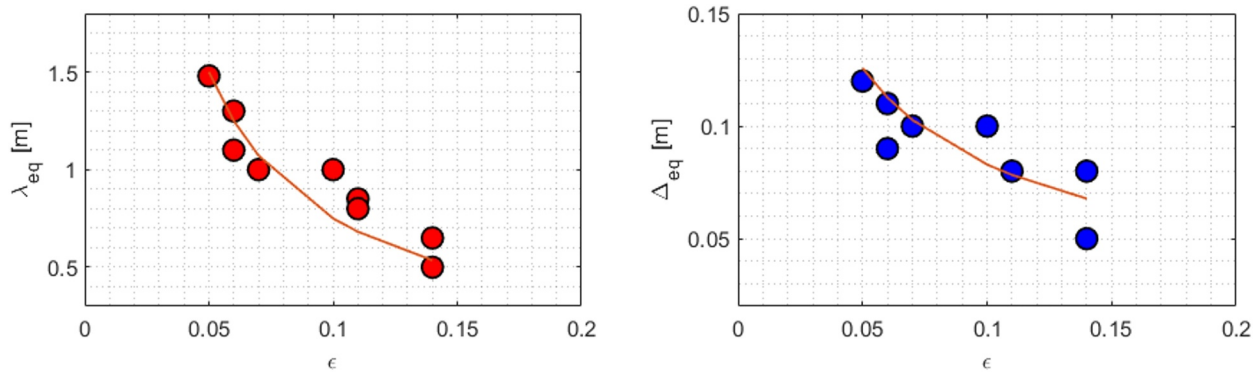

Figure 5. Dune wavelength (λ) and height (Δ) evolution as a function of ε. Solid lines represent the two scaling functions.

height Δ_{eq}, are found to be around 1.3 and 0.11 m, respectively, for low nonlinearities. As the wave nonlinearity increases, both parameters decrease significantly. Grain diameter and flow velocity are two of the variables that affect dune geometry. Additionally, it is regulated by the flow depth, which is a frequently utilized variable due to its ease of use and practicality (Bradley & Venditti, 2017). In this study, we suggest two scaling equations that relate water depth and a function that depends on ε to dune height and wavelength:

$$\Delta = hf(\varepsilon)$$

$$\lambda = hg(\varepsilon)$$

where h is the water depth and $f(\varepsilon) = \frac{1}{12\varepsilon^{0.6}}$ and $g(\varepsilon) = \frac{0.3}{\varepsilon}$ are dimensionless functions that depends on the wave nonlinearity.

3.2. Mean Flow, Turbulent Intensities and Reynolds Shear Stress

The instantaneous horizontal and vertical velocities (u_i, w_i) measured by the UB-Lab 2C at 20 Hz are expressed as the sum of time-averaged velocity (over 5 s, i.e., over 100 instantaneous profiles), $\overline{u}$ and $\overline{w}$ and fluctuating component $u' = u_i - \overline{u}$ and $w' = w_i - \overline{w}$ following the Reynolds averaged Navier Stokes (RANS) framework.

$$\overline{u} = \frac{1}{n}\sum_{i=1}^{n} u_i \quad ; \quad \overline{w} = \frac{1}{n}\sum_{i=1}^{n} w_i \tag{7}$$

Figure 6 displays the contour maps and selected profiles of the mean horizontal flow velocities $\overline{u}$ along migrating dunes in equilibrium for three experiments (T_{A7}, T_{A8} and T_{A9}). These three selected experiments correspond to combined flow tests with the same oscillation frequency but with different wave steepness ε. Multiplying the dune migration velocity C by the elapsed time allows the conversion of time to dimensionless dune wavelength in equilibrium λ_{eq}. Figure 6 illustrates three distinct key aspects that have already been shown and thoroughly discussed by Naqshband et al. (2014).

The first significant characteristic is associated with a zone of flow acceleration at the dune stoss side, where the highest horizontal velocities are above the dune crest. The highest downstream velocities are present just over the crest of the dune in test TA9 (Figure 6c). The second feature corresponds to a flow reversal region situated at the lee side of the migrating dune. The formation of a centimetric internal boundary layer, which begins on the stoss region and ends at the breakpoint of the dune, is the third main feature.

A first-order description of the three experiments shows a qualitatively comparable flow field with a well-developed recirculation cell on the dune lee side. In detail, it appears that the size of this recirculation zone increases for low incident waves (Test TA7). This result suggests a relationship between wave steepness and the extent of the recirculation region. Therefore, the recirculation zone is larger for low amplitude waves, that is, low U_{cf} values.

21699011, 2025, 6, Downloaded from https://agupubs.onlinelibrary.wiley.com/doi/10.1029/2023JF007623 by Universitaet De Caen Normandie, Wiley Online Library on [10/06/2025]. See the Terms and Conditions (https://onlinelibrary.wiley.com/terms-and-conditions) on Wiley Online Library for rules of use; OA articles are governed by the applicable Creative Commons License

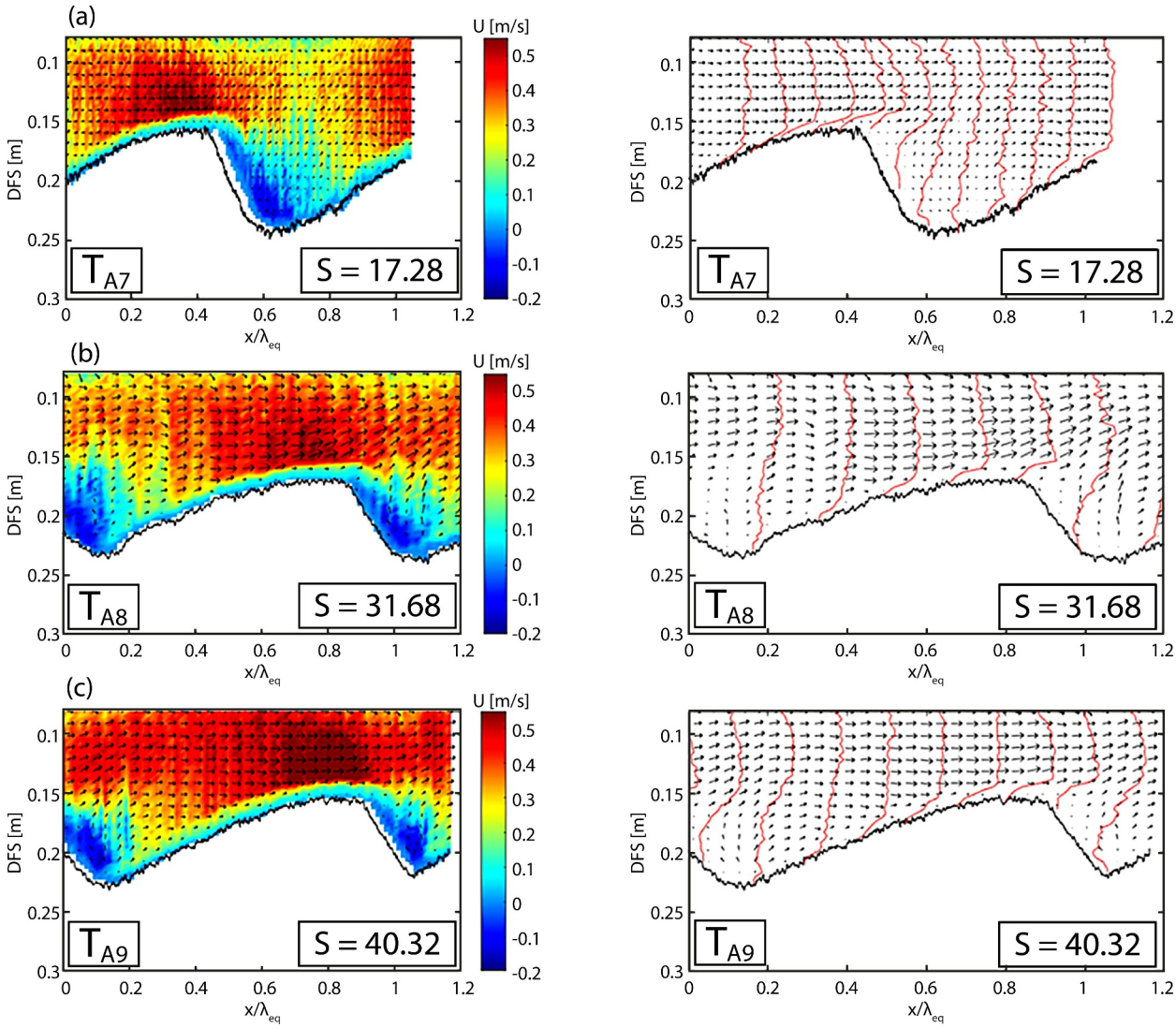

Figure 6. Contour maps and selected profiles of the mean horizontal velocity ($\overline{u}$[m/s]). DFS, Distance From Surface. (a) Low nonlinearity; test T_{A7}, (b) intermediate nonlinearity; test T_{A8}, (c) high nonlinearity; test T_{A9}. The flow direction is from left to right. The solid line shows the dune profile and the arrows represent the mean velocity field $V(\overline{u},\overline{w})$.

The effects of topography on the mean vertical flow are seen in Figure 7 through the time-averaged vertical velocity field $\overline{w}$. Generally, the time-averaged vertical velocity $\overline{w}$ reveals similar general patterns across the three selected tests. The main feature that can be clearly seen is the presence of negative vertical velocities toward the bed in the lee side region, which indicates the impact of flow separation, and positive vertical velocities over the stoss side of the dune, which illustrates the topographic forcing of the combined flow.

The mean horizontal turbulent intensity I_u defined in Equation 8 for the same three selected tests (TA7, TA8 and TA9) is shown in Figure 8, left column. Qualitatively, similar behavior was observed for all experiments. Generally, the shape of the distribution of turbulence intensity is similar to findings from previous research on flow over mobile and fixed 2D dunes when pure unidirectional flow is present (Fernandez et al., 2006; Naqshband et al., 2014). High amounts of turbulence are observed within the reattachment region and along the separation zone shear layer.

$$I_u = \sqrt{\left[\frac{1}{n}\sum_{i=1}^{n}(u')2\right]} \tag{8}$$

21699011, 2025, 6, Downloaded from https://agupubs.onlinelibrary.wiley.com/doi/10.1029/2023JF007623 by Universitaet De Caen Normandie, Wiley Online Library on [10/06/2025]. See the Terms and Conditions (https://onlinelibrary.wiley.com/terms-and-conditions) on Wiley Online Library for rules of use; OA articles are governed by the applicable Creative Commons License

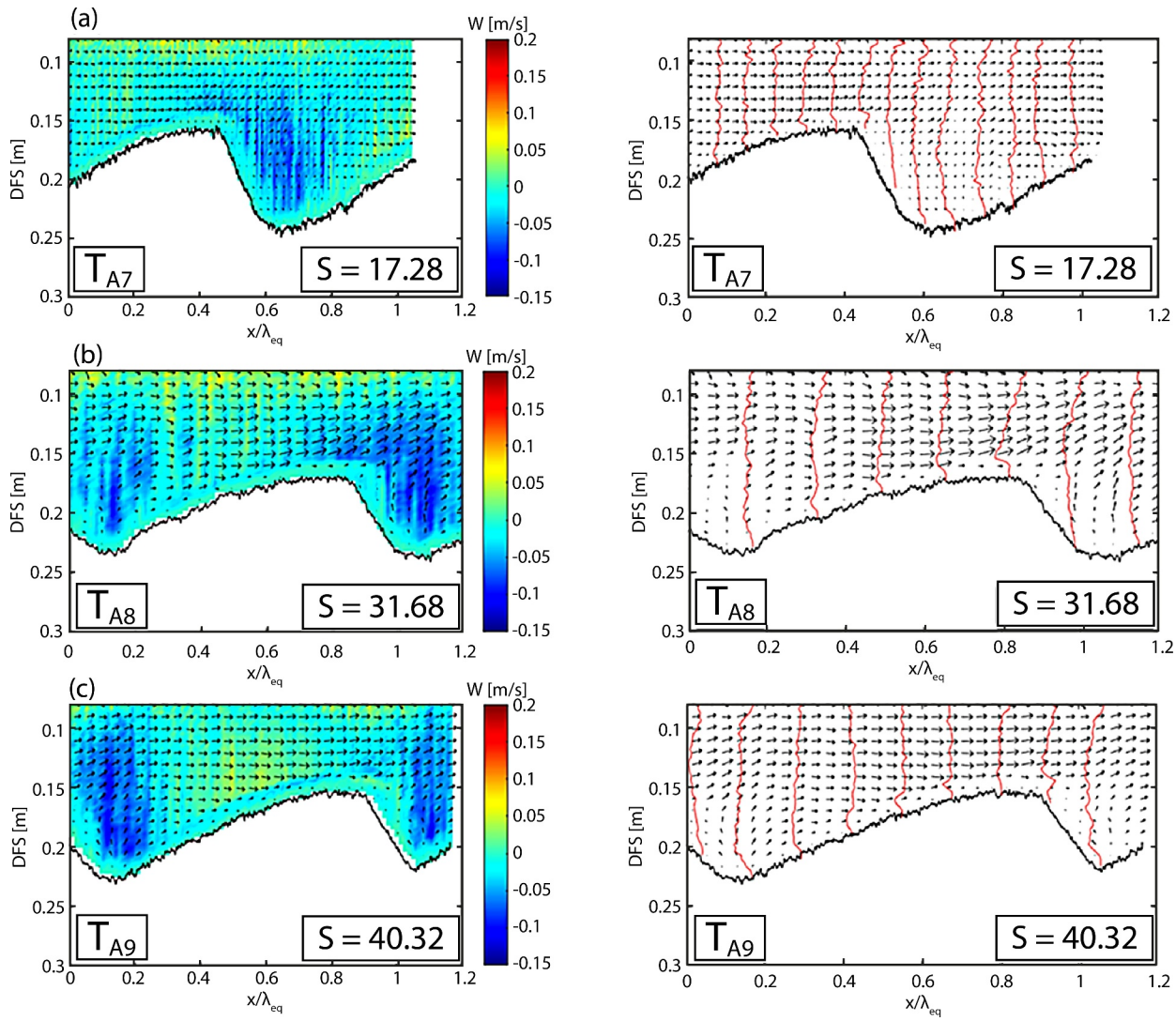

Figure 7. Contour maps and selected profiles of the mean horizontal velocity ($\overrightarrow{w}$ [m/s]). DFS, Distance From Surface as well as flow velocity magnitude and direction (black arrows) (a) low nonlinearity; test T_{A7}, (b) intermediate nonlinearity; test T_{A8}, (c) high nonlinearity; test T_{A9}. The solid line shows the dune profile and the arrows represent the mean velocity field $V(\overline{u},\overline{w})$.

Flow features were further investigated from the spatial distribution of the second-order statistics based on the Reynolds shear stress as it is an important parameter for sediment transport over mobile beds. The following formula was used to calculate the Reynolds shear stress (τ_{uw}) above the migrating dune:

$$\overline{u'w'} = \frac{1}{N}\sum_{i=1}^{N}(u_i - \overline{u})(w_i - \overline{w}) \qquad \tau_{uw} = -\rho\overline{u'w'} \tag{9}$$

where ρ is the fluid density and τ_{uw} is the Reynolds shear stress, and is shown in contour maps (Figure 8, right column). Similar behavior can be observed for the three selected tests, with high values of τ_{uw} extending further downstream and upstream of the recirculation region in test T_{A7} than in test T_{A8} and T_{A9}. This means that the generation of a large dune induces more critical changes in the flow structure and Reynolds stresses near the reattachment zone.

21699011, 2025, 6, Downloaded from https://agupubs.onlinelibrary.wiley.com/doi/10.1029/2023JF007623 by Universitaet De Caen Normandie, Wiley Online Library on [10/06/2025]. See the Terms and Conditions (https://onlinelibrary.wiley.com/terms-and-conditions) on Wiley Online Library for rules of use; OA articles are governed by the applicable Creative Commons License

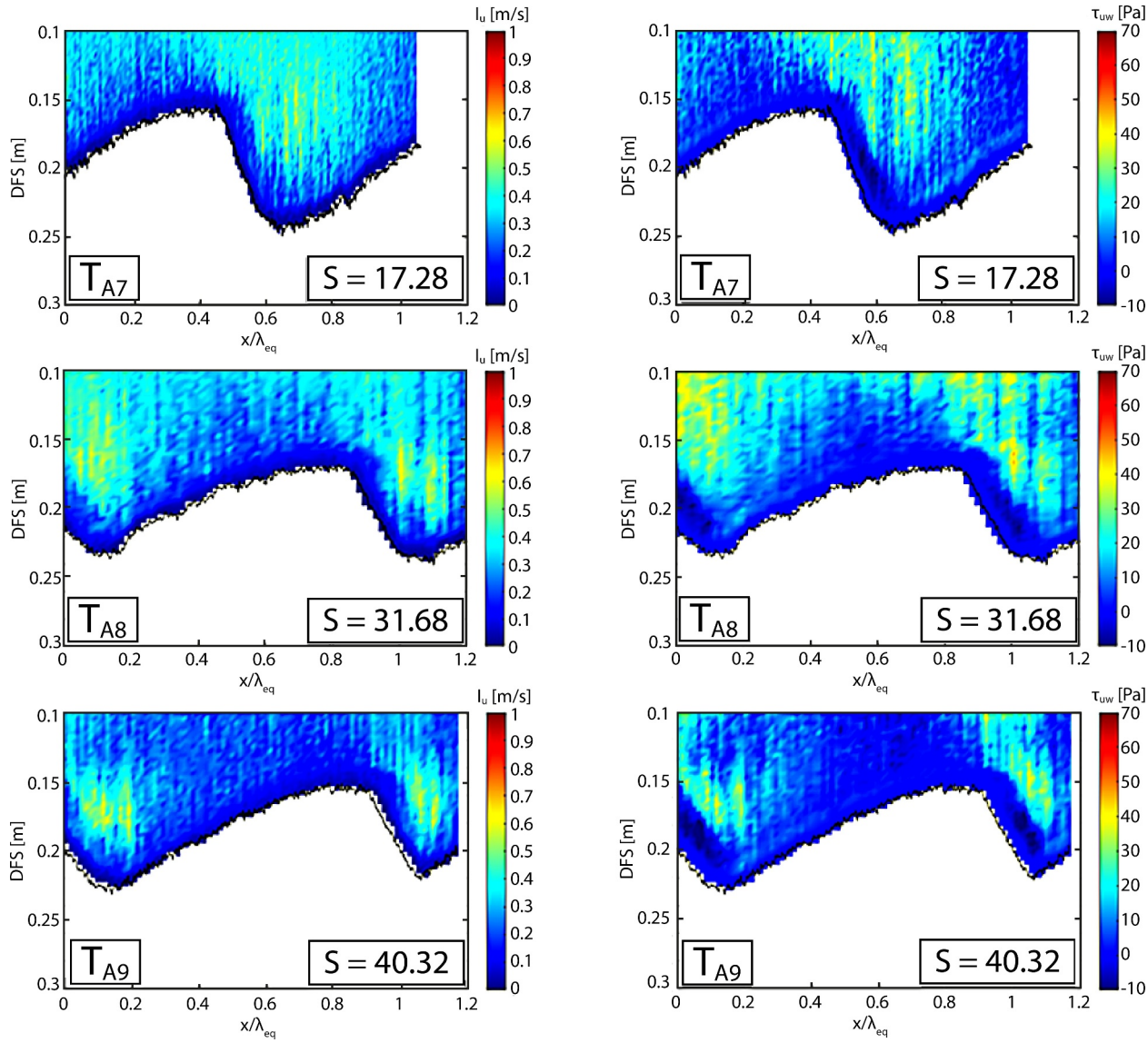

Figure 8. Left column, contour maps and selected profiles of the streamwise turbulence intensity (I [m/s]). Low nonlinearity; test T_{A7}, intermediate nonlinearity; test T_{A8}, high nonlinearity; test T_{A9}. Right column, contour maps and selected profiles of the Reynolds shear stress (τ_{uw} [Pa]). Low nonlinearity; test T_{A7}, intermediate nonlinearity; test T_{A8}, high nonlinearity; test T_{A9}. The flow direction is from left to right and the solid line shows the dune profile. DFS, Distance From Surface.

3.3. Skewness and Kurtosis of the Streamwise Velocity

To further investigate the streamwise flow component, higher order moments related to velocity temporal evolution have been investigated. Third- and fourth-order moments, that is, skewness μ_3 and kurtosis μ_4, are used in this study to quantify the deviation from a Gaussian distribution. Quantitatively, μ_3 and μ_4 reflect, respectively, the asymmetry and the peakedness of the temporal distribution of the horizontal velocity component. The statistical moments are calculated as follows:

$$\mu_3 = N^{1/2}\frac{\sum_{i=1}^{N}(u(t)-\tilde{u})^3}{\left(\sum_{i=1}^{N}\left((u(t)-\tilde{u})^2\right)^{3/2}\right)} \quad (10)$$

21699011, 2025, 6, Downloaded from https://agupubs.onlinelibrary.wiley.com/doi/10.1029/2023JF007623 by Universitaet De Caen Normandie, Wiley Online Library on [10/06/2025]. See the Terms and Conditions (https://onlinelibrary.wiley.com/terms-and-conditions) on Wiley Online Library for rules of use; OA articles are governed by the applicable Creative Commons License

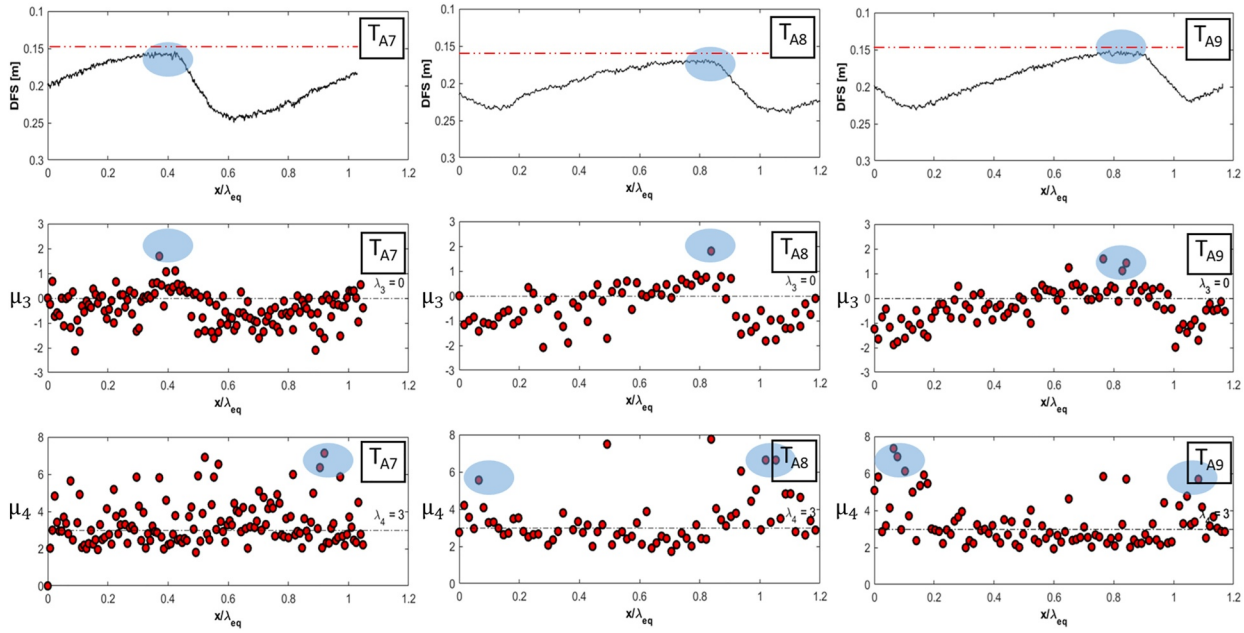

Figure 9. DFS: Distance From Surface. The spatial evolution of μ_3 and μ_4 for three selected tests (T_{A4}, T_{A5} and T_{A6}). The blue added spots correspond to the crest, the location of maxima of the kurtosis and the skewness. The two horizontal dashed lines $\mu_3 = 0$ and $\mu_4 = 3$ correspond to the thresholds of a Gaussian distribution. The red dash-dotted line represents where the temporal velocity calculations were made.

$$\mu_4 = N \frac{\sum_{i=1}^{N} (u(t) - \tilde{u})^4}{\left(\sum_{i=1}^{N} \left((u(t) - \tilde{u})^2 \right)^2 \right)} \tag{11}$$

where the temporal mean velocity over every 5 s is represented by $\tilde{u}$ and $N = 100$ represents the number of samples. In the case of a Gaussian process $\mu_3 = 0$ and $\mu_4 = 3$ are normally expected. Figure 9 displays higher order moments related to the horizontal velocity for three distinct wave steepness (T_{A7}, T_{A8} and T_{A9}). Temporal velocity calculations were made 0.01 m away from the dune crest.

Generally, both kurtosis and skewness deviate substantially from the Gaussian predicted values and are closer to the Gaussian values throughout the mid—stoss region. These deviations can be attributed to the bottom irregularities and to the rise in nonlinear effects associated with wave propagation in shallow waters (Abroug et al., 2020). The skewness has a local maximum on top of the dune and a local minimum on the lee side of the dune. The locations of the dune crest and the skewness appear to coincide perfectly. However, the kurtosis does not have a maximum on top of the dune; rather, the bus has a local maximum on the lee side. This result is qualitatively similar to that found in Trulsen et al. (2020), who experimentally studied velocity and surface elevation statistics of long-crested irregular water surface waves propagating over a shoal. With increasing wave nonlinearity, the skewness and the kurtosis of the streamwise velocity still have the same trend.

Figure 10 shows the relationship between skewness and kurtosis for all studied cases. The majority of streamwise velocities (i.e., more than 85%) exhibit moderate values of skewness and kurtosis, roughly lying between $\mu_3 \in [-1, 1]$ and $\mu_4 \in [2, 5]$. Furthermore, several negatively skewed streamwise velocities are shown in Figure 10, which can be attributed to an increase in second-order effects in shallow regions. This finding is consistent with that of Song and Wu (2000), who showed theoretically that in shallow water locations, the deviation of horizontal velocity statistics from the Gaussian process is more significant.

4. Discussion

In the present experiments, the exposure of a sand bed to combined wave-and-current flows under intermediate depth ($0.5 < kh < 2$, Fr = 0.32) resulted in the formation of asymmetric high-angle dunes with steep lee-side

21699011, 2025, 6, Downloaded from https://agupubs.onlinelibrary.wiley.com/doi/10.1029/2023JF007623 by Universitaet De Caen Normandie, Wiley Online Library on [10/06/2025]. See the Terms and Conditions (https://onlinelibrary.wiley.com/terms-and-conditions) on Wiley Online Library for rules of use; OA articles are governed by the applicable Creative Commons License

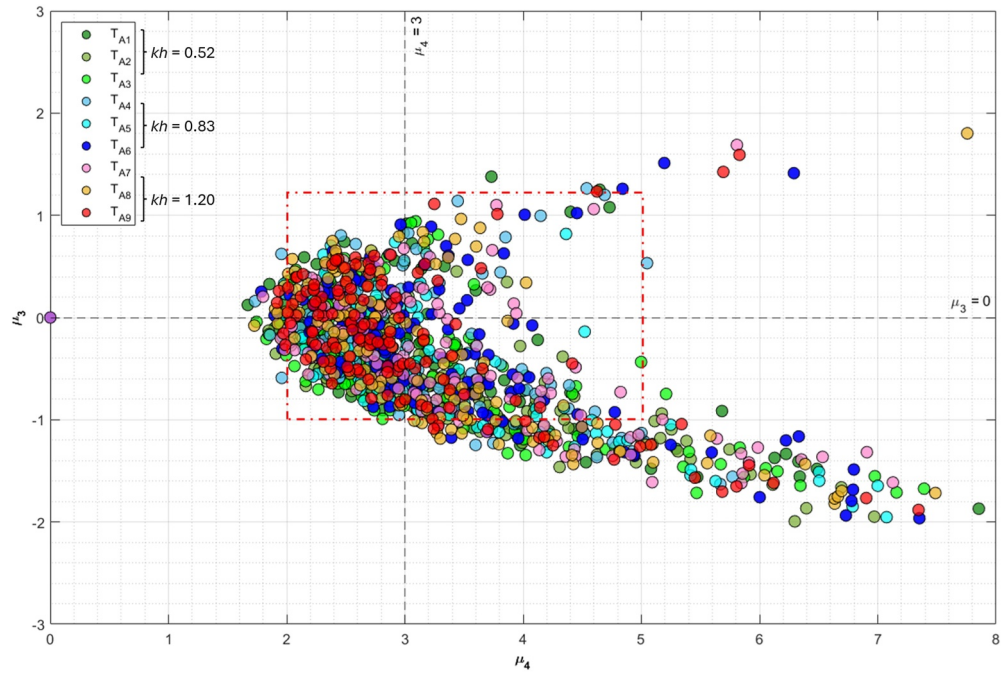

Figure 10. Relationship between skewness and kurtosis in different studied cases. The vertical ($\mu_3 = 0$) and the horizontal ($\mu_4 = 3$) dashed lines correspond to the thresholds of a Gaussian distribution. 85% of the skewness and kurtosis values are situated inside the red dash-dotted rectangle.

slipface at the angle of repose (~30°), producing a permanent zone of flow separation and showing some interaction with the water surface (Kwoll et al., 2016, 2017; Lefebvre et al., 2016). The generated bedforms are thus representative of relatively shallow, tide-dominated, wave-influenced environments, such as shallow subtidal and intertidal sandflats in bays and estuaries. They might also be considered as an analog of megaripples found in shallow tidal shelves as superimposed bedforms on tidal sandwaves (Bellec et al., 2019; Passchier & Kleinhans, 2005).

Although these environments are subject to reversing (sometimes rotating) tidal currents, it was found in the experiments that the time needed to reach a dynamic equilibrium is in the order of one to 2 hrs. This suggests that the bedforms are sufficiently small and reactive to adapt their morphology to transient flow conditions (Reesink et al. (2018) during the tidal cycle or in response to a change in the wave conditions.

The simulation of combined flow showed that superimposed waves accelerate the equilibrium process, which is due to the increase in the combined flow velocity U_{cf}. Moreover, the experiments illustrated that, as the wave nonlinearity increases, both dune height and wavelength decrease significantly. The decrease in dune dimensions can be explained by the increase in fluid excursion and maximum velocity produced by the addition of waves. This conclusion is consistent with findings made by Pedocchi and Garcia (2009), who demonstrated experimentally in the case of purely oscillatory flows that for waves with maximum orbital velocities $U_{\mathrm{wm}} < 0.5$ m/s, the size of ripples decreases with the increase of U_{wm}.

Bradly and Vendetti compiled a data set of dune dimensions (height and wavelength) from both flume experiments (22 flume experiments, 282 observations) and field observations (24 field studies, 382 observations). Using this data compilation, they established a power low (Equation 13) that describes the relationship between the height and the wavelength of subaqueous dunes propagating under current only conditions. Figure 11 shows that our experimental data are slightly higher than those provided by Bradley and Venditti (2017). We can consequently conclude that the form ratio of our dunes was significantly altered by the impact of regular waves. We propose a comparable power law (Equation 13) which allows for the description of wavelength and height under combined flow conditions.

$$\Delta = 0.0513\lambda^{0.77} \tag{12}$$

21699011, 2025, 6, Downloaded from https://agupubs.onlinelibrary.wiley.com/doi/10.1029/2023JF007623 by Universitaet De Caen Normandie, Wiley Online Library on [10/06/2025]. See the Terms and Conditions (https://onlinelibrary.wiley.com/terms-and-conditions) on Wiley Online Library for rules of use; OA articles are governed by the applicable Creative Commons License

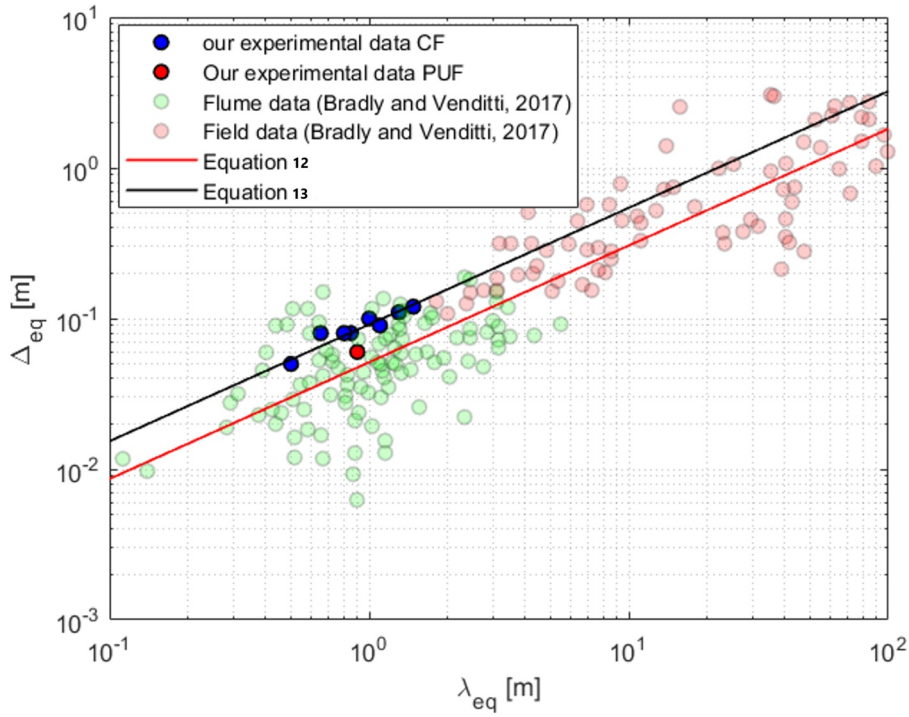

Figure 11. Dune height plotted as a function of wavelength. PUF, pure unidirectional flow; CF, combined flow.

$$\Delta = 0.0913\lambda^{0.77} \tag{13}$$

The physical unit of the constant in both equations is $m^{0.23}$.

Another important observation is that combined flow conditions tend to reduce the three-dimensionality (or sinuosity) of the dune crests compared with current-only flow conditions. Dune crest sinuosity is stronger for current-only and low-wave amplitude tests and decreases as the wave steepness increases. This finding is in accordance with that found in Lacy et al. (2007), who experimentally demonstrated that higher ratios of current to wave energy created more three dimensional bed forms. Similar observations of straight-crested wave-influenced megaripples and more sinuous current megaripples were made by Bellec et al. (2019) on the shallow shelf of the western Barents Sea. Figure 12 illustrates how the wave nonlinearity affects dune asymmetry.

This topographical response to flow versus combined forcing could be partly explained by how much the flow reverses over time. In other words, typical wave-alone conditions have periodic flow reversal. Adding current to the flow reduces and eliminates the flow reversal, especially in the case of low wave amplitude tests. Consequently, symmetric flow conditions, that is, high amplitude combined flow tests, will naturally lead to symmetric deformation (2D dunes). The asymmetric behavior for current-dominated flow conditions will modify the shape of the bedforms by favoring the development of bed perturbation and the emergence of transverse instabilities.

Flow measurements were carried out using UB-Lab 2C, an acoustic velocity profiler newly developed by Ubertone. The flow investigations showed some key aspects that have already been shown and thoroughly discussed by Naqshband et al. (2014) who studied mobile sand dunes migrating in the presence of unidirectional flows. A relationship between wave steepness and the extent of the recirculation region was found. Lower wave amplitude, that is, lower U_{cf} values, implies a larger recirculation zone. This conclusion is consistent with that found in Hamed et al. (2015), who demonstrated experimentally that flow reversal does not occur for high Reynolds unidirectional flow.

The calculation of the time-averaged Reynolds stress revealed additional flow dynamics from the spatial distribution of the second-order statistics. Near the bottom, negative Reynolds stress was found. Hudson et al. (1996), Naqshband et al. (2014), and Hamed et al. (2015) found similar Reynolds stress features at lower Re.

21699011, 2025, 6, Downloaded from https://agupubs.onlinelibrary.wiley.com/doi/10.1029/2023JF007623 by Universitaet De Caen Normandie, Wiley Online Library on [10/06/2025]. See the Terms and Conditions (https://onlinelibrary.wiley.com/terms-and-conditions) on Wiley Online Library for rules of use; OA articles are governed by the applicable Creative Commons License

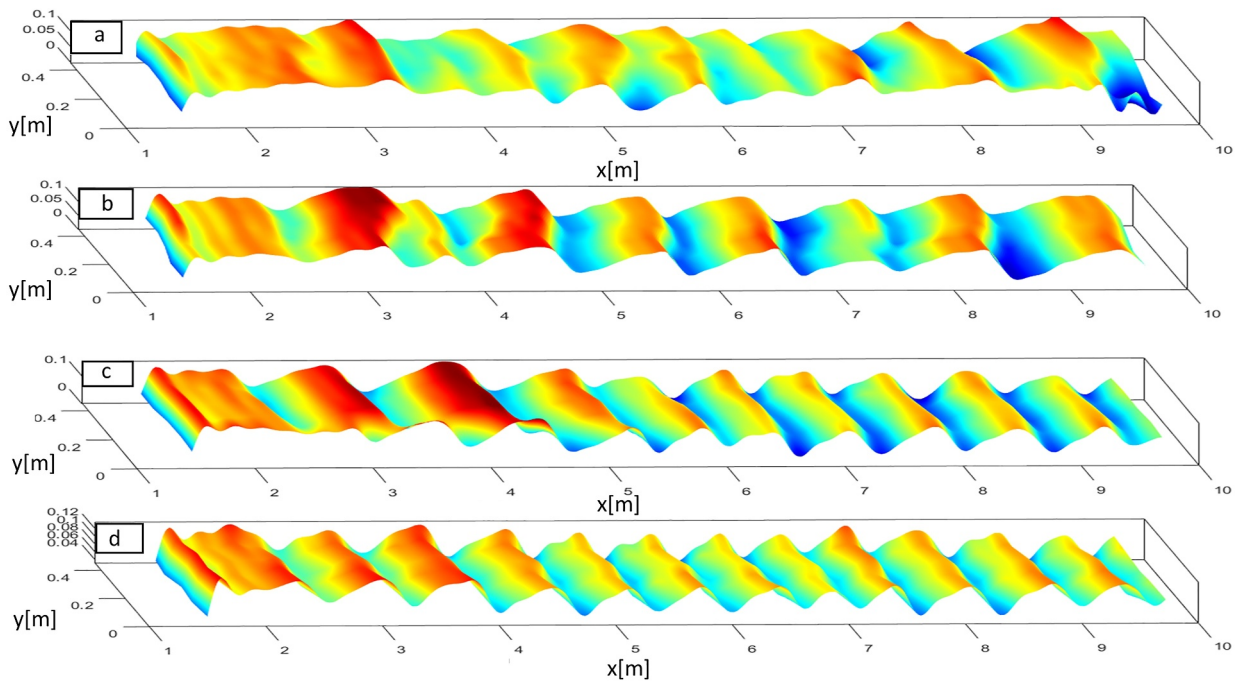

Figure 12. Topography spatial evolution of the migrating dunes after 2.5 hr (in the equilibrium state) of measurements in (a) unidirectional flow condition T_A, (b) combined flow condition with low wave amplitude T_{A7}, (c) combined flow condition with intermediate wave amplitude T_{A8}, (d) combined flow condition with high wave amplitude T_{A9}.

According to Hudson et al. (1996) and Hamed et al. (2015), the negative values toward the bottom are an artifact of employing a cartesian coordinate system rather than a curvilinear coordinate system.

Furthermore, higher order moments related to the streamwise velocity were calculated to assess the flow's non-Gaussian behavior over migrating dunes. One of the primary goals was to determine whether there is a relationship between the experimental values of skewness and kurtosis. Cristelli et al. (2012) demonstrated that this relationship is either a parabolic relation near the Gaussian region or a power low relation for high moments values. In our study, it was demonstrated that a parabolic link was found between experimental values of skewness and kurtosis. This feature has previously been discovered in numerous domains of physics, including plasma physics (Labit et al., 2007), meteorology (Alberghi et al., 2002), and oceanography (Sura & Sardeshmukh, 2008). In contrast to the aforementioned domains, earthquake data (Cristelli et al., 2012) and extreme wave dynamic data (Abroug et al., 2022) exhibit a power low relationship.

5. Summary and Perspectives

We have conducted an experimental study of the topography and flow properties over migrating dunes in the presence of combined flows. The temporal development of dunes was studied under unidirectional (0.5 m/s) and combined wave-and-current flow conditions with oscillation frequencies varying between 0.5 and 1 Hz and with regular wave steepness varying between $\varepsilon = 0.05$ and $\varepsilon = 0.14$. It was found that the temporal development path of dune growth has qualitatively the same general trend regardless of the wave steepness. The main difference between different tests is that dunes reach equilibrium faster for higher combined flow velocities. Experimental evidence has quantitatively shown that the dune's height and wavelength decrease linearly as the wave steepness increases.

Moreover, the flow field above migrating dunes was investigated using the UB-Lab 2C, an acoustic velocity profiler developed by Ubertone. First order and second order statistics, including horizontal velocity, vertical velocity, turbulence and Reynolds shear stress, were studied for several scenarios. The primary hydrodynamic characteristics observed in the migrating dune were mostly consistent with findings from early studies that only examined unidirectional flows. Additionally, it was found that in experiments with low wave steepness, the recirculation region size was larger. To further investigate the velocity field, the deviation from Gaussian statistics

21699011, 2025, 6, Downloaded from https://agupubs.onlinelibrary.wiley.com/doi/10.1029/2023JF007623 by Universitaet De Caen Normandie, Wiley Online Library on [10/06/2025]. See the Terms and Conditions (https://onlinelibrary.wiley.com/terms-and-conditions) on Wiley Online Library for rules of use; OA articles are governed by the applicable Creative Commons License

21699011, 2025, 6, Downloaded from https://agupubs.onlinelibrary.wiley.com/doi/10.1029/2023JF007623 by Universitaet De Caen Normandie, Wiley Online Library on [10/06/2025]. See the Terms and Conditions (https://onlinelibrary.wiley.com/terms-and-conditions) on Wiley Online Library for rules of use; OA articles are governed by the applicable Creative Commons License

was studied using third and fourth order moments. It was demonstrated that non-Gaussian statistics for the horizontal velocity field were triggered by the abrupt depth change. It was found that the peak skewness is on top of the dune's crest but the peak kurtosis is located around the down slope of the dune.

Furthermore, tide-dominated coastal environments are characterized by reversing bi-directional currents. The time needed for the experimental dunes to reach an equilibrium morphology is in the order of 2 hr, which is shorter than a half-tidal cycle. Thus, it can be reasonably assumed that the simulated morphologies can develop in the natural environment during the ebb or the flood. Modeling the response of dunes to reversing currents is of outermost importance and should be investigated in further experiments, as well as the influence of waves propagating against the unidirectional current.

The present experimental results can be used for validating numerical models of turbulent flows in order to explore the flow field for wider ranges of parameters in the presence of combined flows and over large bottom roughness such as dunes.

Data Availability Statement

The topography and flow raw data of the 10 tests used in this work are available in Abroug et al. (2024).

Acknowledgments

This study was carried out as part of the "Modelling of marine Dunes: Local and Large-scale evolutions in an OWF context (MODULLES)" project. We thank Stéphane Fischer and Marie Burckbuchler of the UBERTONE company for providing technical support concerning the UB-Lab 2C device. The authors wish also to express their gratitude to the Normandy region for its financial support.

References

Abroug, I., Abcha, N., Jarno, A., & Marin, F. (2020). Laboratory study of non-linear wave-wave interactions of extreme focused waves in the nearshore zone. *Natural Hazards and Earth System Sciences*, *20*(12), 3279–3291. https://doi.org/10.5194/nhess-20-3279-2020

Abroug, I., Abcha, N., & Pierre, W. (2024). The topography and flow raw data of the ten tests used [Dataset]. *Mendeley Data, V1*. https://doi.org/10.17632/3vbmz58ch8.1

Abroug, I., Matar, R., & Abcha, N. (2022). Spatial evolution of skewness and kurtosis of unidirectional extreme waves propagating over a sloping beach. *Journal of Marine Science and Engineering*, *10*(10), 1475. https://doi.org/10.3390/jmse10101475

Alberghi, S., Maurizi, A., & Tampieri, F. (2002). Relationship between the vertical velocity skewness and kurtosis observed during sea-breeze convection. *Journal of Meteorology and Climatology*, *41*(8), 885–889. https://doi.org/10.1175/1520-0450.(2002)041<0885:RBTVVS>2.0.CO;2

Andreotti, B., Claudin, P., Devauchelle, O., Duràn, O., & Fourrière, A. (2012). Bedforms in a turbulent stream: Ripples, Chevrons and Antidunes. *Journal of Fluid Mechanics*, *690*, 94–128. https://doi.org/10.1017/jfm.2011.386

Arnott, R. W., & Southard, J. B. (1990). Exploratory flow-duct experiments on combined-flow bed configurations, and some implications for interpreting storm-event stratification. *Journal of Sedimentary Research*, *2*, 211–219. https://doi.org/10.1306/212F9156-2B24-11D7-8648000102C1865D

Ashley, G. M. (1990). Classification of large-scale subaqueous bedforms: A new look at an old problem; SEPM bedforms and bedding structures. *Journal of Sedimentary Petrology*, *60*, 160–172. https://doi.org/10.2110/jsr.60.160

Baas, J. H. (1993). *Dimensional analysis of current ripples in recent and ancient depositional environments*. PhD Thesis. Utrecht University. 199.

Barrie, J. V., & Conway, K. W. (2014). Seabed characterization for the development of marine renewable energy on the Pacific Margin of Canada. *Continental Shelf Research*, *83*, 45–52. https://doi.org/10.1016/j.csr.2013.10.016

Bellec, V. K., Bøe, R., Bjarnodottir, L. R., Albresten, J., Dolan, M., Chand, S., et al. (2019). Sandbanks, sandwaves and Megaripples on spitsbergenbanken, Barents sea. *Marine Geology*, *416*, 105998. https://doi.org/10.1016/j.margeo.2019.105998

Best, J. (2005). The fluid dynamics of river dunes: A review and some future research directions. *Journal of Geophysical Research*, *110*(F4), 1–2. https://doi.org/10.1029/2004JF000218

Blom, A., Ribberink, J. S., & De Vriend, H. J. (2003). Vertical sorting in bed forms: Flume experiments with a natural and a Trimodal sediment mixture. *Water Resources Research*, *39*, 2. https://doi.org/10.1029/2001WR001088

Blott, S. J., & Pye, K. (2001). Gradistat: A grain size distribution and statistics package for the analysis of unconsolidated sediments. *Earth Surface Processes and Landforms*, *26*(11), 1237–1248. https://doi.org/10.1002/esp.261

Bradley, R. W., & Venditti, J. G. (2017). Reevaluating dune scaling relations. *Earth-Science Reviews*, *165*, 356–376. https://doi.org/10.1016/j.earscirev.2016.11.004

Bridge, J. S., & Best, J. L. (1988). Flow, sediment transport and bedform dynamics over the transition from dunes to upper-stage plane beds: Implications for the formation of Plana Laminae. *Sedimentology*, *35*, 753–764. https://doi.org/10.1111/j.1365-3091.1988.tb01249.x

Catano-Lopera, Y. A., Abad, K. D., & Garcia, M. H. (2009). Characterization of bedform morphology generated under combined flows and currents using wavelet analysis. *Ocean Engineering*, *39*(9–10), 617–632. https://doi.org/10.1016/j.oceaneng.2009.01.014

Catano-Lopera, Y. A., & Garcia, M. H. (2006). Geometry and migration characteristics of bedforms under waves and currents. Part 1: Sandwave morphodynamics. *Coastal Engineering*, *53*, 9–780. https://doi.org/10.1016/j.coastaleng.2006.03.007

Chatterjee, B. S., Mazumder, B. S., & Ghosh, S. (2018). Turbulence characteristics of wave-blocking phenomena. *Applied Ocean Research*, *75*, 15–36. https://doi.org/10.1016/j.apor.2018.03.011

Couldrey, A. J., Benson, T., Knaapen, M. A. F., Marten, K. V., & Whitehouse, J. S. R. (2020). Morphological evolution of a Barchan dune migrating past an offshore wind farm foundation. *Earth Surface Processes and Landforms*, *45*(12), 4–2896. https://doi.org/10.1002/esp.4937

Cristelli, M., Zaccaria, A., & Pietronero, L. (2012). Universal relation between Skewness and Kurtosis in complex dynamics. *Physical Review*, *85*(6), 066108. https://doi.org/10.1103/PhysRevE.85.066108

Dumas, S., & Arnott, R. W. C. (2006). Origin of hummocky and Swaley cross-stratification. The controlling influence of unidirectional current strength and aggradation rate. *Geology*, *3*(12), 1073–1076. https://doi.org/10.1130/G22930A.1

Duràn Vinent, O., Andreotti, B., Claudin, P., & Winter, C. (2019). A unified model of ripples and dunes in water and planetary environments. *Nature Geoscience*, *12*(5), 345–350. https://doi.org/10.1038/s41561-019-0336-4

Engel, P., & Lau, Y. L. (1980). Friction factor fort wo-dimensional dune roughness. *Journal of Hydraulic Research*, *18*(3), 213–225. https://doi.org/10.1080/00221688009499548

Fernandez, R. L., Best, J., & Lopez, F. (2006). Mean flow, turbulence structure, and bed form superimposition across the ripple-dune transition. *Water Resources Research*, *42*, 5. https://doi.org/10.1029/2005WR004330

Frouriere, A., Claudin, P., & Andreotti, B. (2010). Bedforms in a turbulent stream: Formation of ripples by primary linear instability and of dunes by nonlinear pattern coarsening. *Journal of Fluid Mechanics*, *649*, 287–328. https://doi.org/10.1111/sed.12129

Hamed, A. M., Kamdar, A., Castillo, L., & Chamorro, L. P. (2015). Turbulent boundary layer over 2D and 3D large-scale wavy walls. *Physics of Fluids*, *27*(10), 106601. https://doi.org/10.1063/1.4933098

Hudson, J. D., Dykhno, L., & Hanratty, T. J. (1996). Turbulence production in flow over a wavy wall. *Experiments in Fluids*, *20*(4), 257–265. https://doi.org/10.1007/BF00192670

Jones, K. R., & Traykovski, P. (2019). Interaction of superimposed Megaripples and dunes in a tidally energetic environment. *Journal of Coastal Research*, *35*(5), 948–958. https://doi.org/10.2112/JCOASTRES-D-18-00084.1

Kleinhans, M. G. (2004). Sorting in grain flows at the lee side of dunes. *Earth-Science Reviews*, *65*(1–2), 75–102. https://doi.org/10.1016/S0012-8252(03)00081-3

Kwoll, E., Venditti, J. G., Bradley, R. W., & Winter, C. (2016). Flow structure and resistance over subaquaeous high- and low-angle dunes. *Journal of Geophysical Research: Earth Surface*, *121*(3), 545–564. https://doi.org/10.1002/2015JF003637

Kwoll, E., Venditti, J. G., Bradley, R. W., & Winter, C. (2017). Observations of coherent flow structures over subaqueous high- and low-angle dunes. *Journal of Geophysical Research: Earth Surface*, *5*(11), 2244–2268. https://doi.org/10.1002/2017JF004356

Labit, B., Furno, I., Fasoli, A., Diallo, A., Müller, S. H., Plyushchev, G., et al. (2007). Universal statistical properties of drift-interchange turbulence in TORPEX Plasmas. *Physical Review Letters*, *98*(25), 255002. https://doi.org/10.1103/PhysRevLett.98.255002

Lacy, R. J., Rubin, D. M., Ikeda, H., Mokudai, K., & Hanes, D. M. (2007). Bed forms created by simulated waves and currents in a large flume. *Journal of Geophysical Research*, *112*(C10). https://doi.org/10.1029/2006JC003942

Lefebvre, A., Paarlberg, A. J., & Winter, C. (2016). Characterising natural bedform morphology and its influence on flow. *Geo-Marine Letters*, *36*(5), 379–393. https://doi.org/10.1007/s00367-016-0455-5

Naqshband, S., Ribberink, J. S., Hurther, D., & Hulscher, S. J. M. H. (2014). Bed load and suspended load contributions to migrating sand dunes in equilibrium. *Journal of Geophysical Research: Earth Surface*, *119*(5), 1043–1063. https://doi.org/10.1002/2013JF003043

Passchier, S., & Kleinhans, M. H. (2005). Observations of sand waves, megaripples and hummocks in the Dutch coastal area and their relation to currents and combined flow conditions. *Journal of Geophysical Research*, *110*, F4. https://doi.org/10.1029/2004JF000215

Pedocchi, F., & Garcia, M. H. (2009). Ripple morphology under oscillatory flow: 1. Prediction. *Journal of Geophysical Research*, *114*(C12), C12014. https://doi.org/10.1029/2009JC005354

Perillo, M. M., Best, J. L., Yokokawa, M., Sekiguchi, T., Takagawa, T., & Garcia, M. H. (2014). A unified model for bedform development and equilibrium under unidirectional, oscillatory and combined-flows. *Sedimentology*, *61*(7), 2063–2085. https://doi.org/10.1111/sed.12129

Reesink, A. J. H., Parsons, D. R., Ashworth, P. J., Best, J. L., Hardy, R. J., Murphy, B. J., et al. (2018). The adaptation of dunes to changes in river flow. *Earth-Science Reviews*, *185*, 1065–1087. https://doi.org/10.1016/j.earscirev.2018.09.002

Schindler, R. J., & Robert, A. (2005). Flow and turbulence structure across the ripple-dune transition: An experiment under mobile bed conditions. *Sedimentology*, *52*(3), 627–649. https://doi.org/10.1111/j.1365-3091.2005.00706.x

Singh, S. K., Raushan, P. K., & Debnath, K. (2018). Combined effect of wave and current in rough bed free surface flow. *Ocean Engineering*, *160*, 20–32. https://doi.org/10.1016/j.oceaneng.2018.04.055

Song, J. B., & Wu, Y. H. (2000). Statistical distribution of water-particle velocity below the surface layer for finite water depth. *Coastal Engineering*, *40*(1), 1–19. https://doi.org/10.1016/S0378-3839(99)00062-9

Southard, J. B. (1991). Experimental determination of bed-form stability. *Annual Review of Earth and Planetary Sciences*, *19*(1), 423–455. https://doi.org/10.1146/annurev.ea.19.050191.002231

Southard, J. B., & Boguchwal, L. A. (1990). Bed configurations unsteady unidirectional water flows: Part 2. Synthesis of flume data. *Journal of Sedimentary Petrology*, *60*(5), 658–679. https://doi.org/10.1306/212F9241-2B24-11D7-8648000102C1865D

Sura, P., & Sardeshmukh, P. D. (2008). A global view of Non-Gaussian SST variability. *Journal of Physical Oceanography*, *38*, 639–647. https://doi.org/10.1175/1007JPO3761.1

Trulsen, K., Raustol, A., Jorde, S., & Rye, L. B. (2020). Extreme wave statistics of long-crested irregular waves over a shoal. *Journal of Fluid Mechanics*, *882*, R2. https://doi.org/10.1017/jfm.2019.861

Vah, M., Jarno, A., Le Bot, S., Ferret, Y., & Marin, F. (2020). Bedload transport and bedforms migration under sand supply limitation. *Environmental Fluid Mechanics*, *20*(4), 1031–1052. https://doi.org/10.1007/s10652-020-09738-6

Van der Mark, C. F., & Blom, A. (2007). *A new and widely applicable bedform tracking tool*. University of twente.

Van der Mark, C. F., Blom, A., & Hulscher, S. M. J. H. (2008). Quantification of variability in bedform geometry. *Journal of Geophysical Research*, *113*(F3), 1–11. https://doi.org/10.1029/2007JF000940

Van Lancker, V., Baeye, M., Montereale Gavazzi, G., King, L., Terseleer, N., & Van den Eynde, D. (2020). Monitoring of the impact of the extraction of marine aggregates, in Casu Sand, in the zone of the Hinder Banks. Report. *Period 1/1 – 31/12 2019 and synthesis of results 2016–2016. Brussels, RBINS-OD Nature*.

Venditti, G., Church, M., & Bennett, S. J. (2005). Morphodynamics of small-scale superimposed sand waves over migrating dune bed forms. *Water Resources Research*, *41*, 10. https://doi.org/10.1029/2004WR003461

Warmink, J. J. (2014). Dune dynamics and roughness under gradually varying flood waves, comparing flume and field observations. *Advances in Geosciences*, *39*, 115–121. https://doi.org/10.5194/adgeo-39-115-2014

Whitmeyer, S. J., & Fitzgerald, D. (2006). Sand waves that impede navigation of inlet navigation channels. In *ERDC/CHL CHETN IV-68*. U.S. Army Engineer Research and Development Center.

Wiberg, P. L., & Sherwood, C. R. (2008). Calculating wave-generated bottom orbital velocities from surface-wave parameters. *Computers & Geosciences*, *34*(10), 1243–1262. https://doi.org/10.1016/j.cageo.2008.02.010

Wren, D. G., Kuhnle, R. A., & Wilson, C. G. (2007). Measurements of the relationship between turbulence and sediment in suspension over mobile sand dunes in a laboratory flume. *Journal of Geophysical Research*, *112*(F3), F03009. https://doi.org/10.1029/2006JF000683

Yokokawa, M., Masuda, F., & Endo, N. (1995). Sand particle movement on migrating combined-flow ripples. *Journal of Sedimentary Research*, *65*, 40–44. https://doi.org/10.1306/D4268018-2B26-11D7-8648000102C1865D

21699011, 2025, 6, Downloaded from https://agupubs.onlinelibrary.wiley.com/doi/10.1029/2023JF007623 by Universitaet De Caen Normandie, Wiley Online Library on [10/06/2025]. See the Terms and Conditions (https://onlinelibrary.wiley.com/terms-and-conditions) on Wiley Online Library for rules of use; OA articles are governed by the applicable Creative Commons License